DALTON
FULL PAPER

Electrochemical behavior of a series of undecatungstozincates monosubstituted by first-row transition metals, $ZnW_{11}M(H_2O)O_{39}^{n-}$ (M = Cr, Mn, Fe, Co, Ni, Cu or Zn)

Long Cheng,[a] Haoran Sun,[b] Baifeng Liu,[a] Jinfu Liu[c] and Shaojun Dong *[a]

[a] *Laboratory of Electroanalytical Chemistry, Changchun Institute of Applied Chemistry, Chinese Academy of Sciences, Changchun 130022, People's Republic of China. E-mail: dongsj@ns.ciac.jl.cn; Fax: +86-431-5689711*
[b] *Department of Chemistry, Jilin University, Changchun 130023, China*
[c] *Department of Chemistry, Northeast Normal University, Changchun 13002, China*

Received 9th March 1999, Accepted 4th June 1999

The electrochemical behavior of a series of undecatungstozincates monosubstituted by first-row transition metals, $ZnW_{11}M(H_2O)O_{39}^{n-}$ (M = Cr, Mn, Fe, Co, Ni, Cu or Zn), was investigated systematically and comparably in aqueous solutions by electrochemical and *in situ* UV-visible-near-IR spectroelectrochemical methods. These compounds exhibit not only successive reduction processes of the addenda atoms (W) in a negative potential range, but some of them also involve redox reactions originating from the substituted transition metals (M) such as the reduction of Fe^{III} and Cu^{II} at less negative potentials and the oxidation of Mn^{II} at a more positive potential. Some interesting results and phenomena, especially of the transition metals, were found for the first time. Moreover, possible reaction mechanisms are proposed based on the experimental results.

1 Introduction

Polyoxometalates (POMs) form a distinctive class of inorganic metal–oxygen cluster compounds which is unique in its topological and electronic versatility and useful in fields as diverse as catalysis, analysis, biochemistry, medicine and material science.[1–3] Among the POM structural types the best known and most important ones are Keggin ($XM_{12}O_{40}^{n-}$) and Dawson ($X_2M_{18}O_{62}^{n-}$) structures, where X is a tetrahedrally co-ordinated heteroatom such as Si or P and M is Mo or W. One of the most important properties of these POM anions is their ability to lose, by increasing the pH to appropriate values, one or several addenda cations and their terminally bound oxo groups, thus forming a so-called "lacunary" anion with a vacancy surrounded by five oxo groups. The lacunary anions can act as unique ligands to accommodate transition metal cations in the vacancies, where the lacunary anionic ligands present pentadentate (as for "octahedral" Mn^{2+}) or tetradentate (as for "square-planar" Cu^{2+}) binding sites.

Transition metal substituted polyoxometalates (TMSPs) have attracted much attention and interest especially in catalysis, because they bear not only some similarities in co-ordination environment and catalytic reactivity to metalloporphyrins and other metal complexes of macrocyclic ligands, but also have some peculiar advantages.[3–6] For example, (i) the overall non-oxidizable inorganic framework of POMs should be highly oxidation resistant and thermally robust; (ii) they can work in both polar and non-polar solvents; (iii) they may show much richer redox chemistry originating from the well known addenda cations of W or Mo as well as the substituted transition metals which may function as catalytic active sites; (iv) important properties (acidity, stability and redox potential, *etc.*) of TMSPs can be adjusted by reduction to heteropolyblues (HPBs), by substitution of selected atoms and by choice of pH range. Consequently, TMSPs have found wide applications, especially in organic catalysis such as epoxidation of olefins,[5,6] hydrocarbon oxidation[7] and aliphatic and aromatic hydroxylation.[6]

Many research groups have reported that a variety of transition metal cations can be enclosed in the vacancies of lacunary POM anions of Keggin or Dawson structures, including Ti,[8a–c] V,[9] Cr,[4a,8d,10,11] Mn,[4b,5,6,8c–e,12,13] Fe,[6,8c–e,10,14b,c] Co,[4c,5,6,8c–e,10] Ni,[6,8c–e] Cu,[6,8c–e,10,12] Zn,[8c–e] Ga,[14a] In,[14a,15] Rh,[14b] Re[16a] and Ru.[7,16b] Most of the previous studies paid much attention to the synthesis, characterization and applications of these TMSPs. As the transition metals are usually the active sites, their redox properties deserve to be investigated in order to understand the reaction mechanisms and to design suitable electrocatalysts. However, they remain to be studied thoroughly and systematically, although a few studies have been reported,[8–11,15,16] and a review published on the electrochemical properties of POMs as electrocatalysts.[3b] Some results were reported recently for a few discrete TMSPs including $PW_{11}Ru$,[17a] $XW_{11}Fe$ (X = Si, Ge, P or As),[17b–e] $SiW_{11}Mn$,[18,19] $P_2W_{17}Fe$[20,21c,d] and $PW_{11}Fe$.[21a,b] To our knowledge, there were no comprehensive electrochemical studies until Bidan and his co-workers[21] reported a comparative electrochemical study of Dawson-type TMSPs, $P_2W_{17}M$ (M = Fe, Cu, Co, Ni or Mn), and their ability electrocatalytically to reduce nitrite.

We have studied the electrochemical behavior and electrocatalytic properties of various POMs and their chemically modified electrodes.[20,22] This article reports comprehensive results for seven anions $ZnW_{11}M$. The redox processes of both addenda atoms (W) and substituted transition metals (M) were studied in detail by electrochemical and *in situ* UV-visible-near-IR spectroelectrochemical methods, and compared with each other and with their saturated parent compound 12-tungstozincate acid $H_6ZnW_{12}O_{40}$. Some interesting results and phenomena are reported here for the first time. The synthesis and some characterization of $ZnW_{11}M$ were reported previously.[8c] In addition, Pope and co-workers[13a] reported recently the presence of high valent manganese in Keggin polyoxotungstates $XW_{11}Mn^{IV}$ (X = Si, B or Zn).

2 Experimental

2.1 Materials

The potassium salts of this TMSP series, $K_nH[ZnW_{11}M(H_2O)O_{39}]\cdot xH_2O$ (abbreviated as $ZnW_{11}M$, M = Cr, Mn, Fe, Co, Ni,

Table 1 Formal potentials of redox waves for a saturated POM ZnW_{12} and seven TMSP $ZnW_{11}M$ (M = Cr, Mn, Fe, Co, Ni, Cu or Zn). All voltammetric measurements were conducted in pH 4.0 buffer solution at a scan rate of 0.1 V s^{-1}

Compound	M-centered	1st W-centered	2nd W-centered	3rd W-centered	4th W-centered
ZnW_{12}	—	—	−0.546	−0.693	−0.894
$ZnW_{11}Cr$	—	−0.401	−0.564	−0.706	−0.902
$ZnW_{11}Mn$	0.929	−0.396	−0.555	−0.703	−0.897
$ZnW_{11}Fe$	−0.167	−0.411	−0.572	−0.715	—
$ZnW_{11}Co$	—	−0.389	−0.550	−0.692	−0.889
$ZnW_{11}Ni$	—	−0.380	−0.553	−0.701	−0.896
$ZnW_{11}Cu$	0.072	−0.384	−0.561	−0.702	—
$ZnW_{11}Zn$	—	−0.396	−0.557	−0.700	−0.894

Cu or Zn) were prepared and characterized according to the literature.[8c] 12-Tungstozincate acid $H_6ZnW_{12}O_{40}$ (denoted as ZnW_{12}) was prepared using a similar procedure to that described by Nomiya and Miwa.[23] All other chemicals were of reagent grade used as received. Buffer solutions were prepared from 0.1 M $NaHSO_4$ (pH 1–4) and 0.1 M NaOAc/HOAc (pH 4–6), and adjusted to desired pH values by 0.2 M NaOH or 0.1 M H_2SO_4. The supporting electrolyte was 0.1 M Na_2SO_4. Doubly distilled deionized water was used to prepare solutions. All solutions were degassed with pure argon for at least 15 min before use.

2.2 Electrochemical measurements

Electrochemical experiments were performed with a CHI 600 voltammetric analyzer (CH instruments, USA) in a conventional three-electrode cell. The working electrodes (WEs) used here were home-made glassy carbon electrodes (GCEs). The surfaces of GCEs were polished with 1.0, 0.3 and 0.05 μm α-Al_2O_3 powder successively and washed ultrasonically in water. A twisted platinum wire was used as the counter electrode (CE), and Ag–AgCl (in saturated KCl solution) as the reference electrode (RE), against which all potentials were measured and reported. Formal potentials (E_f) of redox couples in CVs were estimated as average values of anodic (E_{pa}) and cathodic (E_{pc}) peak potentials, *i.e.* $E_f = (E_{pa} + E_{pc})/2$; peak potential separations, $\Delta E_p = E_{pa} - E_{pc}$.

2.3 Spectroelectrochemical measurements

In situ UV-visible-near-IR spectra were obtained with a Shimadzu 3100 UV-VIS-NIR spectrophotometer (Japan) coupled with an HPD-1A potentiostat/galvanostat (China). A home-made thin-layer spectroelectrochemical cell with adjustable optical path length was employed.[24] Two plates of quartz were used as UV-visible-near-IR spectral windows. The WE was a 100 mesh platinum gauze of 20 × 10 mm woven from 50 μm platinum wire. Two large-area platinum sheets were distributed at both sides of the WE as a CE. A small Ag–AgCl (in saturated KCl solution) electrode was used as an RE.

3 Results and discussion

3.1 General electrochemical behavior

The electrochemical measurement of $ZnW_{11}M$ was mainly conducted in aqueous solutions by cyclic voltammetry. For comparison, the electrochemical reduction of saturated 12-tungstozincate acid ZnW_{12} was obtained since no lacunary anions are known.[1] The series of $ZnW_{11}M$ exhibit not only successive reduction processes of the addenda atoms (W) in a negative potential range, but some of them also involve redox reactions of the substituted transition metals (M) such as the reduction of Fe^{III} and Cu^{II} at less negative potentials and the oxidation of Mn^{II} at a more positive potential. Their voltammetric data are summarized in Table 1. A comprehensive description follows.

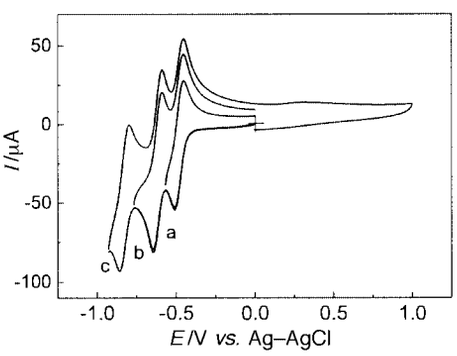

Fig. 1 The CVs of 3.4 mM $H_6ZnW_{12}O_{40}$ in pH 3.06 buffer at 0.1 V s^{-1} with different negative potential limits: (a) −0.57, (b) −0.77 and (c) −0.93 V.

3.1.1 The saturated parent heteropolyanion ZnW_{12}. As shown in Fig. 1, CVs of ZnW_{12} in pH 3.06 buffer consist of three reduction steps with formal potentials of −0.482, −0.618 and −0.829 V respectively. There are no redox waves in the positive potential range. Similar to those of $H_2W_{12}O_{40}^{6-}$,[1] the three redox couples of ZnW_{12} with equal heights are all two-electron reaction processes, consistent with the fact that their potential separations are around 30–40 mV. With increasing pH, E_f of the three two-electron waves becomes more negative, and the first two-electron wave eventually splits into two one-electron waves at *ca.* pH 5.

3.1.2 $ZnW_{11}M$ with electroinactive substituted metals M = Cr, Co, Ni or Zn. Fig. 2 shows CVs of $ZnW_{11}Cr$ (a), $ZnW_{11}Co$ (b), $ZnW_{11}Ni$ (c) and $ZnW_{11}Zn$ (d) in *ca.* pH 3.5 aqueous solutions. $ZnW_{11}Co$, $ZnW_{11}Ni$ and $ZnW_{11}Zn$ exhibit similar well-resolved voltammograms. That for $ZnW_{11}Cr$ is less resolved. In a negative potential range between −0.3 and −0.95 V there are four well defined redox waves originating from the tungsten oxo framework. They are one one-electron and three two-electron transfer processes respectively, evidenced by comparison of peak currents with those known for ZnW_{12}. These properties may be a reflection of the unknown lacunary anion ZnW_{11} (see refs 17(*b*) and 20).

In the positive potential range between +1.0 and −0.3 V, however, no redox waves are observed, suggesting that the four substituted transition metal cations Cr^{III}, Co^{II}, Ni^{II} and Zn^{II} within the lacunary heteropolyanion have no electroactivity under our experimental conditions. For comparison, experiments were also conducted on the electroactivity of the free cations Cr^{3+}, Co^{2+}, Ni^{2+} and Zn^{2+} under the same conditions as for $ZnW_{11}M$. No oxidation processes were observed.

3.1.3 $ZnW_{11}M$ with electroactive substituted metals M = Cu, Fe or Mn. *(A) $ZnW_{11}Cu$.* Fig. 3 shows CVs of 1.8 mM $ZnW_{11}Cu$ at pH 3.5 with different negative potential limits. Three couples of tungsten oxo based reduction appear at negative potentials close to those of $ZnW_{11}M$ (M = Cr, Co, Ni or Zn). The fourth reduction wave is less resolved because of overlap with the hydrogen evolution reaction and is not shown here.

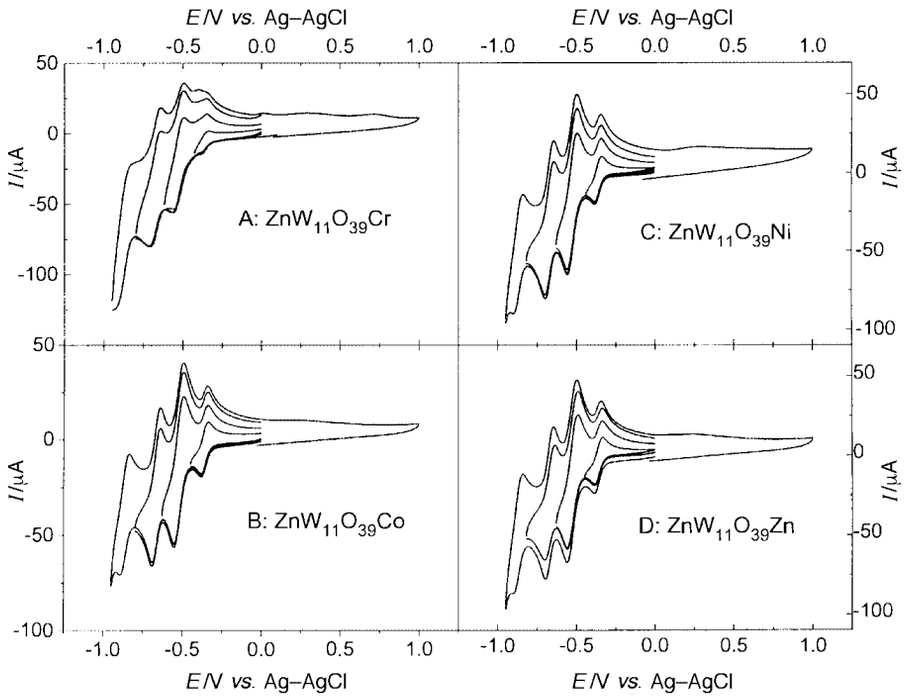

Fig. 2 The CVs of four $ZnW_{11}M$ in pH 3.5 buffer at 0.1 V s^{-1} within different potential ranges: (A) 2.2 mM $ZnW_{11}Cr$, (B) 1.8 mM $ZnW_{11}Co$, (C) 2.1 mM $ZnW_{11}Ni$ and (D) 2.0 mM $ZnW_{11}Zn$.

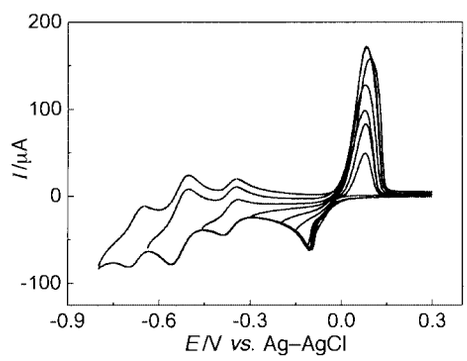

Fig. 3 The CVs of 1.8 mM $ZnW_{11}Cu$ in pH 3.5 buffer at 0.1 V s^{-1} with different negative potential limits: −0.05, −0.10, −0.15, −0.20, −0.30, −0.46, −0.64 and −0.80 V.

Moreover, an unusual redox wave appears in the less negative potential range between 0.2 and −0.3 V. It consists of a broad cathodic peak near −0.1 V and a sharp anodic peak at about 0.1 V. The sharp anodic peak current increases as the switching potential becomes more negative and reaches a maximum value before the onset of tungsten reduction. The unusual redox wave is assigned to reduction and oxidation of the transition metal Cu within $ZnW_{11}Cu$. Bidan and co-workers[21c] also reported a Cu-centered redox wave of Dawson-type $P_2W_{17}Cu$, whose cathodic peak is masked by the first one of the tungsten centers at pH 3. However, in our case the Cu-centered redox wave is well separated from the tungsten ones.

The effect of scan rate on the anodic peak was examined. A freshly polished GCE was preconditioned at −0.2 V for 10 s to ensure an identical extent of reduction. As shown in Fig. 4A, the anodic peak potential shifts positively and the peak current increases linearly with increasing scan rate. This is consistent with a surface-confined reaction. In addition, the very sharp anodic peak indicates that the oxidation corresponds to an anodic stripping process. Moreover, with increasing preconditioning time (Fig. 4B) the anodic peak current increases steadily, while the peak potential shifts positively. These results are similar to that of anodic stripping of free Cu^{2+} ion.[25] It is reasonable to expect that the stability of both the copper-(II) and -(I) cations within $ZnW_{11}Cu$ will be decreased by the five-co-ordinate geometry imposed by the POM framework, favoring reduction to Cu^0 and dissociation.[26] This interpretation is supported by Fig. 5, which shows that the Cu-centered peak currents decrease gradually during a ten-cycle potential sweep. It is indicative of demetallation of $ZnW_{11}Cu$, *i.e.* the copper center separates from its original co-ordinated state, similar to the results for some copper complexes.[27] The W-based redox waves, however, remain unchanged during the continuous potential sweeping, which suggests that the lacunary anion ZnW_{11} formed after the demetallation exhibits similar redox processes to those of $ZnW_{11}Cu$. It means that the W-based redox processes exhibited by the $ZnW_{11}M$ anions indeed reflect the redox behavior of the lacunary anion ZnW_{11}, as anticipated in part 3.1.2.

In conclusion, the copper(II) cation within $ZnW_{11}Cu$ undergoes a two-electron reduction to Cu^0, but the Cu^0 inside the POM skeleton would probably be high in energy, which should favor dissociation and deposition of Cu^0 on the electrode surface (Cu^0/GCE); Cu^0/GCE is reoxidized to Cu^{2+} near the interface between the electrode and solution ($Cu^{2+}{}_{GCE}$). The $Cu^{2+}{}_{GCE}$ probably recombines with the lacunary POM ZnW_{11} to form $ZnW_{11}Cu^{II}$, or diffuses into the bulk solution as free Cu^{2+} ($Cu^{2+}{}_{solution}$). In contrast, it is unknown whether the Cu-centered reduction of $P_2W_{17}Cu$ is a two- or one-electron process.[21c] In our case a plausible Cu-centered reaction mechanism is as given in eqns. (1)–(5).

$$ZnW_{11}Cu^{II} + 2e \longrightarrow ZnW_{11}Cu^0 \quad E_{pc} = ca. -0.1\ V \quad (1)$$

$$ZnW_{11}Cu^0 \longrightarrow ZnW_{11} + Cu^0/GCE$$
Partially decompose (2)

$$Cu^0/GCE - 2e \longrightarrow Cu^{2+}{}_{GCE} \quad E_{pa} = ca.\ 0.1\ V \quad (3)$$

$$ZnW_{11} + Cu^{2+}{}_{GCE} \longrightarrow ZnW_{11}Cu^{II}$$
Probably recombine (4)

$$Cu^{2+}{}_{GCE} \longrightarrow Cu^{2+}{}_{solution}$$
Diffuse into the bulk solution (5)

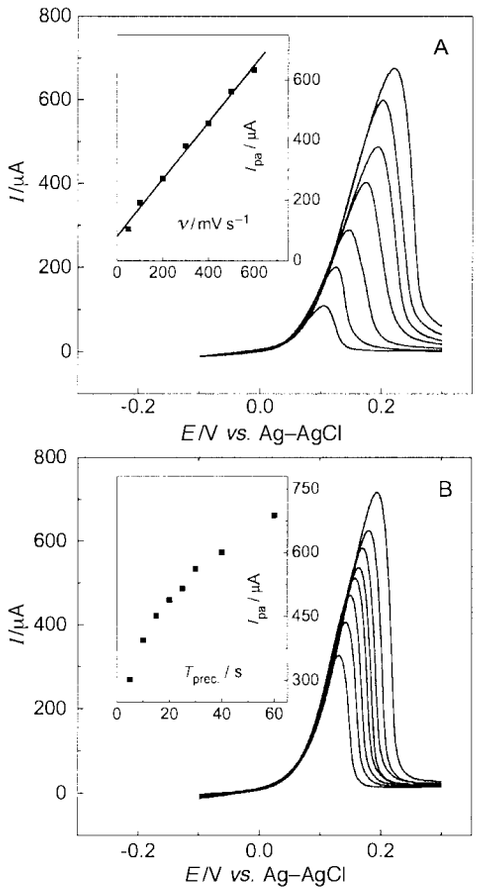

Fig. 4 (A) The CVs after preconditioning at −0.2 V for 10 s at different scan rates: 0.05, 0.1, 0.2, 0.3, 0.4, 0.5 and 0.6 V s^{-1}. The insert shows a linear relationship of the anodic peak currents *vs.* scan rates. (B) The CVs at 0.1 V s^{-1} after preconditioning at −0.2 V for different periods: 5, 10, 15, 20, 25, 30, 40 and 60 s. The insert shows the relationship of the anodic peak currents *vs.* the preconditioning time. The solution is 1.8 mM $ZnW_{11}Cu$ in pH 3.5 buffer.

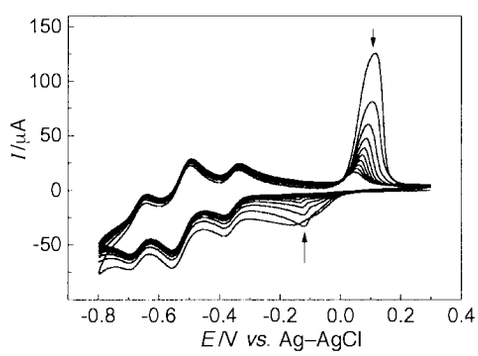

Fig. 5 The CVs of 1.8 mM $ZnW_{11}Cu$ in pH 3.5 buffer at 0.1 V s^{-1} recorded during continuous potential sweeping for ten cycles.

(B) $ZnW_{11}Fe$. In contrast with $ZnW_{11}M^{II}$ (M = Co, Ni, Cu, Zn or Mn (see below)), $ZnW_{11}Fe^{III}$ exhibits relatively ill defined tungsten-based redox waves, as does $ZnW_{11}Cr^{III}$ (Fig. 6B). The difference in charges of M^{III} (M = Fe or Cr) and M^{II} (M = Co, Ni, Cu, Zn or Mn) apparently plays some role. Nevertheless, $ZnW_{11}Fe$ undergoes tungsten-based redox processes at potentials close to those of $ZnW_{11}M^{II}$.

As shown in Fig. 6(A), it is obvious that a new one-electron redox wave occurs with E_f of −0.14 V and ΔE_p of 118 mV. It corresponds to a quasi-reversible $Fe^{III/II}$ couple of $ZnW_{11}Fe$, which is similar to other Fe-containing TMSPs.[20,21] However, we found that the iron cathodic peak current decreased to one-third after a complete redox cycle. It implies that the whole iron redox process may not be a simple $ZnW_{11}Fe^{III/II}$ couple.

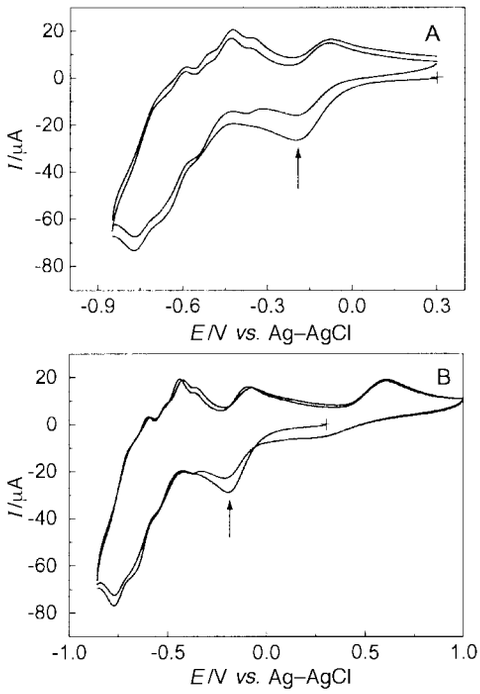

Fig. 6 (A) The CVs of 1.7 mM $ZnW_{11}Fe$ in pH 3.3 buffer for two cycles in a negative potential range between 0.3 and −0.85 V. (B) The CVs of the same solution as (A) in an enlarged potential range between 1.0 and −0.86 V with a first scan to negative potentials. Scan rate: 0.1 V s^{-1}.

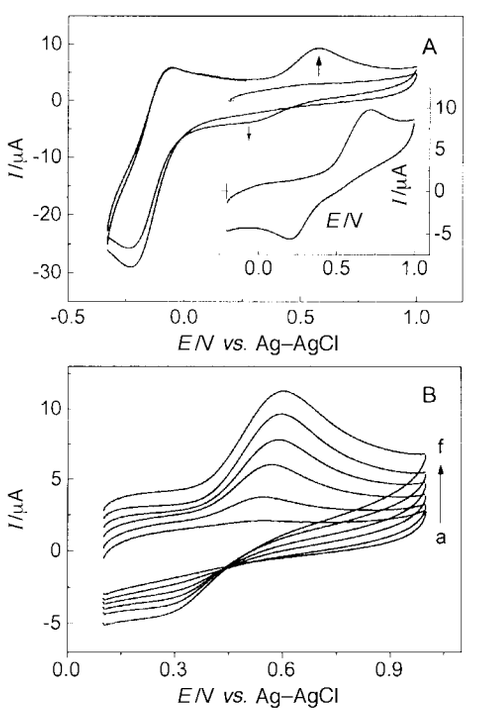

Fig. 7 (A) The CVs of 1.7 mM $ZnW_{11}Fe$ in pH 3.3 buffer with a first scan to 1.0 V and then back to −0.33 V. The insert is a CV of 0.5 mM $FeSO_4$ in pH 3.06 buffer. (B) The CVs of 1.7 mM $ZnW_{11}Fe$ in pH 3.3 buffer in a positive potential range between 0.1 and 1.0 V after preconditioning at −0.2 V for different periods: (a) 0, (b) 1, (c) 3, (d) 5, (e) 10 and (f) 20 s. Scan rate: 0.1 V s^{-1}.

When the upper-limit potential is extended to +1.0 V (Fig. 6B) another anodic peak is present at 0.60 V with a weaker cathodic counterpart around 0.20 V on the reverse scan. Fig. 7(A) shows that this behavior is induced only after scanning the cathodic peak at −0.14 V. It is independent of reduction of the tungsten framework. Furthermore, Fig. 7(B) shows CVs of

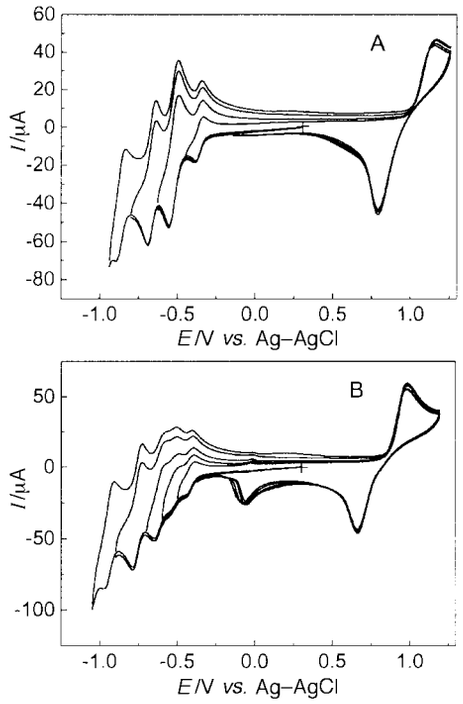

Fig. 8 (A) The CVs of 1.5 mM $ZnW_{11}Mn$ in pH 3.5 buffer with different negative potential limits: −0.45, −0.63, −0.80 and −0.94 V. (B) The CVs of 1.4 mM $ZnW_{11}Mn$ in pH 4.8 buffer with different negative potential limits: −0.50, −0.60, −0.70, −0.90 and −1.05 V. Scan rate: 0.1 V s^{-1}.

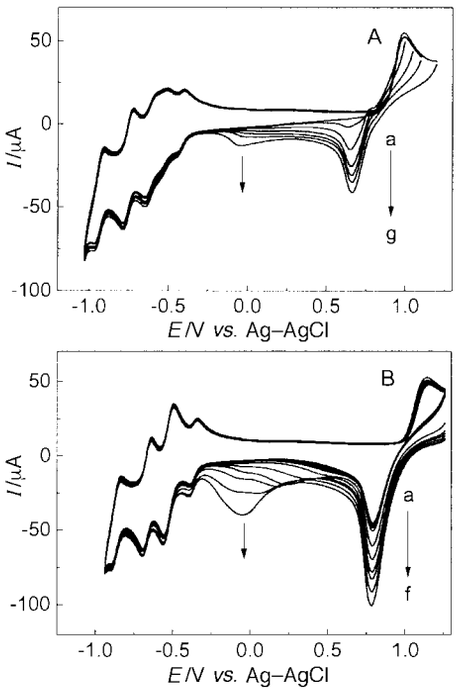

Fig. 9 (A) The CVs of 1.4 mM $ZnW_{11}Mn$ in pH 4.8 buffer with different positive potential limits: 0.85, 0.90, 0.95, 1.0, 1.05, 1.1 and 1.2 V. (B) The CVs of 1.5 mM $ZnW_{11}Mn$ in pH 3.5 buffer after preconditioning at 1.05 V for different periods: 5, 10, 15, 20, 30 and 40 s. Scan rate: 0.1 V s^{-1}.

$ZnW_{11}Fe$ in a positive potential range after first preconditioning at −0.20 V where $ZnW_{11}Fe^{III}$ is reduced to $ZnW_{11}Fe^{II}$ for different periods. A new redox couple grows gradually and its peak currents increase steadily with preconditioning time. Therefore, the new couple of redox waves at positive potentials must involve Fe and may result from a chemical reaction accompanying the $ZnW_{11}Fe^{III/II}$ redox process.

The insert of Fig. 7(A) shows a CV of free Fe^{2+} cation under the same conditions as for $ZnW_{11}Fe$. The behavior is similar to that observed for $ZnW_{11}Fe$ at positive potentials and suggests that Fe^{2+} is responsible for the new redox couple. This unusual feature has not been noted before.

(C) $ZnW_{11}Mn$. The compound $ZnW_{11}Mn$ in pH 3.5 buffer also exhibits a single one- and three two-electron W-based redox waves at negative potentials, as shown in Fig. 8(A). A new redox couple is observed at positive potentials of 1.17 V for oxidation and 0.79 V for reduction, which must correspond to an Mn-centered reaction.[4b,5,6,8c–e,12,13] When the pH is increased, the peak potentials of both the W- and Mn-centered redox waves of $ZnW_{11}Mn$ shift negatively, indicating that all of them are accompanied by protonation. Fig. 8(B) shows CVs of 1.4 mM $ZnW_{11}Mn$ in pH 4.8 buffer. It can be seen that the first two-electron wave at pH 3.5 (Fig. 8A) has split into two one-electron waves at pH 4.8, which is a common feature of POMs under higher pH conditions.[1,3b] Additionally, a new cathodic peak occurs at −0.082 V and the Mn-centered redox wave in Fig. 8(A) moves negatively to 1.0 (oxidation) and 0.66 V (reduction). The CVs in Fig. 8(B) are similar to previous observations.[13a]

The effect of different upper-limit potentials on the new cathodic peak was investigated. Fig. 9A demonstrates that the appearance of the new cathodic peak is closely related to the magnesium oxidation state. Moreover, the new cathodic peak does appear in CVs of 1.5 mM $ZnW_{11}Mn$ in pH 3.5 buffer after preconditioning at a more positive potential of 1.05 V for several minutes, as shown in Fig. 9(B). It can be seen that as the preconditioning time increases the new cathodic peak grows in gradually, the peak current of the first Mn-centered reduction at 0.79 V increases simultaneously and the W-based redox processes remain unchanged.

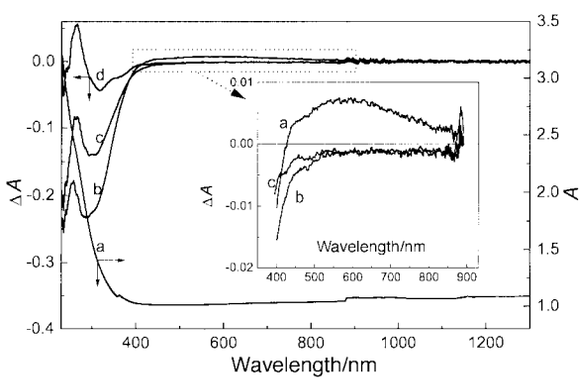

Fig. 10 *In situ* UV-visible-near-IR spectral changes of 1.6 mM $ZnW_{11}Fe^{III}$ in pH 3.3 buffer obtained by subtraction of the spectra after sequential electrolysis at potentials of (b) −0.25, (c) 0.20 and (d) 0.55 V from the original spectrum of $ZnW_{11}Fe^{III}$ (curve a).

3.2 Spectroelectrochemical characterization of $ZnW_{11}M$

3.2.1 $ZnW_{11}Fe$. Fig. 10 gives some *in situ* UV-visible-near-IR spectroelectrochemical results of 1.6 mM $ZnW_{11}Fe^{III}$ in pH 3.3 buffer. Curve a (with bottom *X* axis and right *Y* axis) is a UV-visible-near-IR spectrum of $ZnW_{11}Fe^{III}$ after electrolysis at 0.30 V, which is identical to that of the original solution at open circuit as no reactions occur at 0.30 V. In contrast, curves (b), (c) and (d) (with bottom *X* axis and left *Y* axis) are depicted as *in situ* UV-visible-near-IR subtraction spectra in order to highlight the spectral changes, obtained by subtracting the spectra after sequential electrolysis at potentials of −0.25, 0.20 and 0.55 V from the original one of $ZnW_{11}Fe^{III}$ (curve a), respectively.

Some spectral changes occur (curve b) after potential stepping from 0.30 to −0.25 V where the one-electron reduction of $ZnW_{11}Fe^{III}$ occurs, according to the above CV results. First, an obvious decrease in absorption within the UV range (less than

400 nm) where ligand-to-metal charge transfer (LMCT) bands are expected to appear. This decrease is consistent with the fact that the interaction between Fe and oxygen atoms must decrease after reduction of $ZnW_{11}Fe^{III}$ to $ZnW_{11}Fe^{II}$. Secondly, a broad weak increase in absorption can be seen in the visible range between *ca.* 430 and 900 nm, which is enlarged and shown independently in the insert of Fig. 10 for clarity. The broad absorption band around 600 nm is also characteristic of a d–d band of Fe^{II}. Thirdly, there are almost no spectral changes in the near IR range, where intervalence charge transfer (IVCT) bands of mixed valence heteropolyanions are expected to occur. It is implied that no W-centered reduction happens after electrolysis at −0.25 V. In conclusion, the first reduction of $ZnW_{11}Fe^{III}$ at −0.25 V can be assigned to Fe-centered reduction to form $ZnW_{11}Fe^{II}$ consistent with the above *in situ* spectroelectrochemical results.

After potential stepping from −0.25 to 0.20 V (curve c) the LMCT band in the UV spectral range increases; and the d ⟶ d transfer band in the visible spectral range decreases (see the insert) in comparison with curve b. This is consistent with the oxidation of $ZnW_{11}Fe^{II}$ at 0.20 V to form $ZnW_{11}Fe^{III}$. However, it should be noted that the final spectrum after electrolysis at 0.20 V does not come back to the original one because the curve c is far away from zero. This result indicates that the redox process of $ZnW_{11}Fe^{III/II}$ is not a completely reversible reaction and thus there may be a coupled homogeneous chemical reaction following it. Moreover, after potential stepping from 0.20 to 0.55 V (curve d), comparing with curve c, the LMCT band increases continuously and approaches more the original one but is not yet identical. The absorption values at 310 and 350 nm are still smaller whereas that at 270 nm is larger than the initial ones. The fact that the spectra cannot come back to its original suggests that an irreversible process is occurring after the redox reaction of $ZnW_{11}Fe^{III/II}$.

In addition, the thin-layer cyclic voltammograms and corresponding cyclic voltabsorptograms (not shown here) support the above *in situ* UV-visible-near-IR spectroelectrochemical results. The spectroelectrochemical results also agree well with the results of cyclic voltammetry (see above).

According to the above results from both the electrochemical and *in situ* spectroelectrochemical experiments, a possible reaction mechanism involving an electrochemically induced demetallation is proposed for the Fe-related redox processes of $ZnW_{11}Fe^{III}$ in an order similar to Fig. 6B, eqns. (6)–(11). The

$$[ZnW_{11}Fe^{III}]^{7-} + e \longrightarrow [ZnW_{11}Fe^{II}]^{8-} \quad E_{pc} = -0.20\ V \quad (6)$$

$$[ZnW_{11}Fe^{II}]^{8-} \longrightarrow [ZnW_{11}]^{10-} + Fe^{2+}$$
Partially decompose (7)

$$[ZnW_{11}Fe^{II}]^{8-} - e \longrightarrow [ZnW_{11}Fe^{III}]^{7-} \quad E_{pa} = -0.08\ V \quad (8)$$

$$Fe^{2+} - e \longrightarrow Fe^{3+} \quad E_{pa} = 0.61\ V \quad (9)$$

$$Fe^{3+} + e \longrightarrow Fe^{2+} \quad E_{pc} = 0.20\ V \quad (10)$$

$$Fe^{3+} + [ZnW_{11}]^{10-} \longrightarrow [ZnW_{11}Fe^{III}]^{7-}$$
Partially recombine (11)

ligands on Fe are omitted for clarity, but would not invalidate the mechanism.

3.2.2 $ZnW_{11}Mn$. Spectroelectrochemical experiments were also conducted in 1.0 mM $ZnW_{11}Mn^{II}$ pH 4.6 buffer. Fig. 11 shows some typical *in situ* UV-visible-near-IR subtraction spectra to emphasize their spectral changes, obtained by subtraction of the spectra after sequential electrolysis at potentials of 1.0 (b), 0.55 (c) and 0.30 V (d) from the original spectrum of $ZnW_{11}Mn^{II}$ (curve a). After potential stepping from 0.30 to 1.0

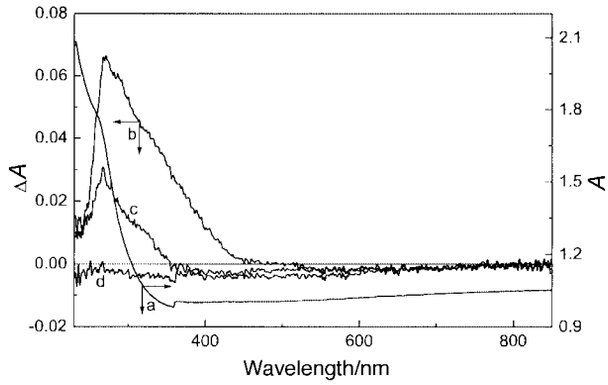

Fig. 11 *In situ* UV-visible-near-IR spectral changes of 1.0 mM $ZnW_{11}Mn^{II}$ in pH 4.6 buffer obtained by subtraction of the spectra after sequential electrolysis at potentials of (b) 1.0, (c) 0.55 and (d) 0.30 V from the original spectrum of $ZnW_{11}Mn^{II}$ (curve a).

V (curve b), the absorption values of the LMCT band in the UV spectral range increase since the spectral changes are positive. This is in line with the fact that the interaction between manganese and oxygen atoms must increase after oxidation of $ZnW_{11}Mn^{II}$ to higher-valent manganese $ZnW_{11}Mn^{IV}(OH)$ according to the results of Pope and co-workers.[13a]

After potential stepping from 1.0 to 0.55 V (curve c) the spectral changes of the LMCT band decrease in comparison with curve b, but do not restore the original one since the ΔA values are significantly different from zero. Such a result implies that $ZnW_{11}Mn^{IV}$ is partially reduced to $ZnW_{11}Mn^{III}$, not to $ZnW_{11}Mn^{II}$.[13a] Moreover, after potential stepping from 0.55 to 0.30 V (curve d), the LMCT band is nearly identical with the original one since the ΔA values are very close to zero. This result suggests that $ZnW_{11}Mn^{III}$ is reduced to $ZnW_{11}Mn^{II}$ and the original state reached again after a series of Mn-centered redox processes. Therefore, the Mn-centered redox process is a closed cycle, in other words the manganese always stays coordinated within $ZnW_{11}Mn$ during its redox reaction without any dissociation, which is different from the $ZnW_{11}Cu$ and $ZnW_{11}Fe$ cases.

Based on our experimental results from the spectroelectrochemistry and cyclic voltammetry (see above), a provisional Mn-centered reaction mechanism of $ZnW_{11}Mn^{II}$ is proposed by referring to some results of Pope and co-workers,[13] eqns. (12)–(14). The peak potential values are obtained at pH 4.79 (Fig. 8B).

$$ZnW_{11}Mn^{II}(H_2O)^{8-} + 2e \longrightarrow ZnW_{11}Mn^{IV}(OH)^{7-}$$
$$E_{pa} = 0.998\ V \quad (12)$$

$$ZnW_{11}Mn^{IV}(OH)^{7-} - e \longrightarrow ZnW_{11}Mn^{III}(H_2O)^{7-}$$
$$E_{pc1} = 0.66\ V \quad (13)$$

$$ZnW_{11}Mn^{III}(H_2O)^{7-} - e \longrightarrow ZnW_{11}Mn^{II}(H_2O)^{8-}$$
$$E_{pc2} = -0.08\ V \quad (14)$$

4 Concluding remarks

The electrochemical behavior of a series of $ZnW_{11}M$ compounds (M = Cr, Mn, Fe, Co, Ni, Cu or Zn) was investigated systematically by electrochemical and *in situ* UV-visible-near-IR spectroelectrochemical methods. All of the compounds exhibit four couples of successive W-centered reduction processes with similar peak potentials. It is proposed that the W-centered redox processes of $ZnW_{11}M$ might reflect those of its unknown lacunary anion ZnW_{11}. In addition, $ZnW_{11}M$ (M = Cu, Fe or Mn) undergo redox reactions originating at the metals M. The compound $ZnW_{11}Cu^{II}$ exhibits Cu-centered deposition and stripping, $ZnW_{11}Fe^{III}$ an unusual Fe-centered

redox process at positive potentials and $ZnW_{11}Mn$ an oxidation and two reduction processes. Some provisional reaction mechanisms are proposed based on the present experimental results. Further studies are underway in our laboratory.

5 Acknowledgements

Financial support from the National Natural Science Foundation of China is greatly appreciated.

6 References

1 M. T. Pope, *Heteropoly and isopoly oxometalates*, Springer, New York, 1983.
2 M. T. Pope and A. Muller, *Angew. Chem., Int. Ed. Engl.*, 1991, **30**, 34.
3 (*a*) C. L. Hill (Guest editor), *Chem. Rev.*, 1998, **98**, No. 1 (the full book); (*b*) M. Sadakane and E. Steckhan, *Chem. Rev.*, 1998, **98**, 219.
4 D. E. Katsoulis and M. T. Pope, (*a*) *J. Chem. Soc., Chem. Commun.*, 1986, 1186; (*b*) *J. Chem. Soc., Chem. Commun.*, 1989, 1483; (*c*) *J. Am. Chem. Soc.*, 1984, **106**, 2737.
5 C. L. Hill and R. B. Brown, *J. Am. Chem. Soc.*, 1986, **108**, 536.
6 (*a*) D. K. Lyon, W. K. Miller, T. Novet, P. J. Domaille, E. Evitt, D. C. Johnson and R. C. Finke, *J. Am. Chem. Soc.*, 1991, **113**, 7209; (*b*) D. Mansuy, J.-F. Bartoli, P. Battioni, D. K. Lyon and R. C. Finke, *J. Am. Chem. Soc.*, 1991, **113**, 7222.
7 R. Neumann and C. Abu-Gnim, (*a*) *J. Chem. Soc., Chem. Commun.*, 1989, 1324; (*b*) *J. Am. Chem. Soc.*, 1990, **112**, 6025.
8 (*a*) Y. G. Chen and J. F. Liu, *Polyhedron*, 1996, **15**, 3433; (*b*) L. Meng and J. F. Liu, *Transition Met. Chem.*, 1995, **20**, 188; (*c*) J. F. Liu, Y. Wang, Q. H. Yang, Y. G. Chen, M. X. Li, C. G. Liu and S. T. Yang, *Polyhedron*, 1996, **15**, 717; (*d*) J. F. Liu, X. P. Zhang, F. Q. Wang, G. P. Li, Q. H. Yang and J. P. Wang, *Chem. Res. Chin. Univ.*, 1995, **11**, 1; (*e*) J. F. Liu, F. Q. Wang, Y. Wang, Q. H. Yang, W. Wang and X. H. Zhu, *Transition Met. Chem.*, 1995, **20**, 81.
9 E. Codot, M. Fournier, A. Teze and G. Herve, *Inorg. Chem.*, 1996, **35**, 282.
10 J. F. Liu, F. Ortega, P. Sethuraman, D. E. Katsoulis, C. E. Costello and M. T. Pope, *J. Chem. Soc., Dalton Trans.*, 1992, 1901.
11 C. Rong and F. C. Anson, *Inorg. Chem.*, 1994, **33**, 1064.
12 C. M. Tourne, G. F. Tourne, S. M. Malik and T. J. R. Weakley, *J. Inorg. Nucl. Chem.*, 1970, **32**, 3875.
13 (*a*) X. Y. Zhang, M. T. Pope, M. R. Chance and G. B. Jameson, *Polyhedron*, 1995, **14**, 1381; (*b*) X. Y. Zhang, G. B. Jameson, C. J. O'Connor and M. T. Pope, *Polyhedron*, 1996, **15**, 917; (*c*) X. Y. Zhang, C. J. O'Connor, G. B. Jameson and M. T. Pope, *Inorg. Chem.*, 1996, **35**, 30.
14 (*a*) F. Zonnevijlle, C. M. Tourne and G. F. Tourne, *Inorg. Chem.*, 1982, **21**, 2742; (*b*) F. Zonnevijlle, C. M. Tourne and G. F. Tourne, *Inorg. Chem.*, 1982, **21**, 2751; (*c*) R. Contant, M. Abbessi, J. Canny, A. Belhouari, B. Keita and L. Nadjo, *Inorg. Chem.*, 1997, **36**, 4961.
15 W. Sun, H. Liu, J. Kong, G. Xie and J. Deng, *J. Electroanal. Chem. Interfacial Electrochem.*, 1997, **437**, 67; W. Sun, F. Yang, H. Liu, J. Kong, S. Jin, G. Xie and J. Deng, *J. Electroanal. Chem. Interfacial Electrochem.*, 1998, **451**, 49.
16 (*a*) F. Ortega and M. T. Pope, *Inorg. Chem.*, 1984, **23**, 3292; (*b*) C. Rong and M. T. Pope, *J. Am. Chem. Soc.*, 1992, **114**, 2932.
17 (*a*) J. C. Bart and F. C. Anson, *J. Electroanal. Chem. Interfacial Electrochem.*, 1995, **390**, 11; (*b*) J. E. Toth and F. C. Anson, *J. Electroanal. Chem. Interfacial Electrochem.*, 1988, **256**, 361; (*c*) J. E. Toth and F. C. Anson, *J. Am. Chem. Soc.*, 1989, **111**, 2444; (*d*) J. E. Toth, J. D. Melton, D. Cabelli, B. H. J. Bielski and F. C. Anson, *Inorg. Chem.*, 1990, **29**, 1952; (*e*) K. K. Shiu and F. C. Anson, *J. Electroanal. Chem. Interfacial Electrochem.*, 1991, **309**, 115.
18 M. Sadakane and E. Steckhan, *J. Mol. Catal. A*, 1996, **114**, 221.
19 A. Muller, L. Dloczik, E. Diemann and M. T. Pope, *Inorg. Chim. Acta*, 1997, **257**, 231.
20 S. Dong and M. J. Liu, *J. Electroanal. Chem. Interfacial Electrochem.*, 1994, **372**, 95.
21 (*a*) B. Fabre, G. Bidan and M. Laplowski, *J. Chem. Soc., Chem. Commun.*, 1994, 1509; (*b*) B. Fabre and G. Bidan, *J. Chem. Soc., Faraday Trans.*, 1997, 591; (*c*) T. McCormac, B. Fabre and G. Bidan, *J. Electroanal. Chem. Interfacial Electrochem.*, 1997, **425**, 49; (*d*) T. McCormac, B. Fabre and G. Bidan, *J. Electroanal. Chem. Interfacial Electrochem.*, 1997, **427**, 155.
22 S. Dong and B. Wang, *Electrochim. Acta*, 1992, **37**, 11; *J. Electroanal. Chem. Interfacial Electrochem.*, 1992, **328**, 245; S. Dong and W. Jin, *J. Electroanal. Chem. Interfacial Electrochem.*, 1993, **354**, 87; S. Dong, X. Xi and M. Tian, *J. Electroanal. Chem. Interfacial Electrochem.*, 1995, **385**, 227; L. Cheng, X. Zhang, X. Xi, B. Liu and S. Dong, *J. Electroanal. Chem. Interfacial Electrochem.*, 1996, **407**, 97.
23 K. Nomiya and M. Miwa, *Polyhedron*, 1983, **2**, 955.
24 H. R. Sun, S. Y. Zhang, J. Q. Xu, G. Y. Yang and T. S. Shi, *J. Electroanal. Chem. Interfacial Electrochem.*, 1998, **455**, 57.
25 M. A. Baldo, C. Bragato, G. A. Mazzocchin and S. Daniele, *Electrochim. Acta*, 1998, **43**, 3413.
26 (*a*) M. M. Bernardo, P. V. Robandt, R. R. Schroeder and D. B. Rorabacher, *J. Am. Chem. Soc.*, 1989**, 111**, 1224; (*b*) N. M. Villeneuve, R. R. Schroeder, L. Z. Ochrymowycz and D. B. Rorabacher, *Inorg. Chem.*, 1997, **36**, 4475.
27 J. M. Fernandez-G, S. Hernandez-Ortega, R. Cetina-Rosado, N. Macias-Ruvalcaba and M. Aguilar-Martinez, *Polyhedron*, 1998, **17**, 2425.

Paper 9/01846H